Research Article | Vol. 28, No. 13 / 22 June 2020 / Optics Express 19446
Optics EXPRESS

Sub-ppb-level CH_4 detection by exploiting a low-noise differential photoacoustic resonator with a room-temperature interband cascade laser

HUADAN ZHENG,[1] YIHUA LIU,[1] HAOYANG LIN,[1] RUIFENG KAN,[2] PIETRO PATIMISCO,[3] ANGELO SAMPAOLO,[3] MARILENA GIGLIO,[3] WENGUO ZHU,[1] JIANHUI YU,[1,5] FRANK K TITTEL,[4] VINCENZO SPAGNOLO,[3,6] AND ZHE CHEN[1]

[1]*Key Laboratory of Optoelectronic Information and Sensing Technologies of Guangdong Higher Education Institutes, Department of Optoelectronic Engineering, Jinan University, Guangzhou 510632, China*
[2]*State Key Laboratory of Applied Optics, Changchun Institute of Optics, Fine Mechanics and Physics, Chinese Academy of Sciences, Changchun 130033, China*
[3]*PolySense Lab - Dipartimento Interateneo di Fisica, University and Politecnico of Bari, CNR-IFN, Via Amendola 173, Bari, Italy*
[4]*Department of Electrical and Computer Engineering, Rice University, 6100 Main Street, Houston, TX 77005, USA*
[5]*kensomyu@gmail.com*
[6]*vincenzoluigi.spagnolo@poliba.it*

Abstract: An ultra-highly sensitive and robust CH_4 sensor is reported based on a 3.3 μm interband cascade laser (ICL) and a low-noise differential photoacoustic (PAS) cell. The ICL emission wavelength targeted a fundamental absorption line of CH_4 at 2988.795 cm^{-1} with an intensity of 1.08×10^{-19} cm/molecule. The double-pass and differential design of the PAS cell effectively enhanced the PAS signal amplitude and decreased its background noise. The wavelength modulation depth, operating pressure and V-T relaxation promotion were optimized to maximize the sensor detection limit. With an integration time of 90 s, a detection limit of 0.6 ppb was achieved. No additional water or air laser cooling were required and thereby allowing the realization of a compact and robust CH_4 sensor.

© 2020 Optical Society of America under the terms of the OSA Open Access Publishing Agreement

1. Introduction

Methane (CH_4), the primary component of natural gas, is a kind of greenhouse gas with a 100-year global warming potential 25 times that of carbon dioxide [1]. With the booming development of oil and natural gas industry in recent years, there is a need to identify and assess possible environmental and economic consequences associated with gas activities. Rapidly identify and profile CH_4 leaks from facilities will allow operators to quickly narrow down and mitigate probable leaking equipment, reducing the CH_4 emission to atmosphere.

Photoacoustic spectroscopy (PAS) is a powerful tool for trace gas sensing due to its advantages of high sensitivity and selectivity as well as robustness of the detection module [2,3]. The principle of PAS is to detect the acoustic waves generated by the molecules upon absorption of the radiation, whose frequency is resonant with the vibrational or rotational absorption energy levels of the target gas molecule [4]. Commonly used photoacoustic transducers are microphones [5–7], fiber tips [8–10], cantilevers [11–13] and quartz tuning forks [14–21]. Light sources with emission wavelengths ranging from ultraviolet to terahertz have been implemented for PAS gas

#391322 https://doi.org/10.1364/OE.391322
Journal © 2020 Received 25 Feb 2020; revised 28 May 2020; accepted 11 Jun 2020; published 17 Jun 2020

Optics EXPRESS

sensing [22,23]. The PAS signal S can be expressed by the following equation [4]:

$$S \propto \frac{\alpha(\gamma - 1)QCP}{fV} \tag{1}$$

where α is the molecular absorption coefficient, γ is the adiabatic index, Q is the quality factor of the PAS resonator, C is the transducer efficiency, P is the excitation optical power, f is the modulation frequency and V is the PAS cell volume, respectively.

Since the molecular absorption coefficient α in the mid-infrared (MIR) spectral region is orders of magnitude stronger than that in the near infrared (NIR) region [24–28], a higher detection sensitivity can be achieved when operating in the MIR spectral region. Optical sensors based on quantum cascade lasers (QCLs) have been demonstrated in the past decades [29–39]. However, commercially available QCLs are limited to wavelengths longer than 3.7 μm. To cover the 3-4 μm spectral range, where the fundamental absorption bands of the main hydrocarbon gases such as methane (CH_4), ethane (C_2H_6) and propane (C_3H_8) fall, interband cascade lasers (ICLs) [40–44] are the best choice. In addition, the power consumption of ICLs is much lower than the power required to operate QCL sources.

PAS gas sensors employing ICLs have been demonstrated in the past. W. Ren et al. developed a portable low-power QEPAS-based CO_2 isotope sensor using a fiber-coupled 4.35 μm ICL [45]. A. Loh and M. Wolff obtained high resolution spectra of ^{13}C ethane and propane isotopologues using two ICLs [46]. M. Lassen et al. demonstrated a sensor for continuous monitoring of oil contamination in compressed air systems by using a custom made ICL [47]. J. Rouxel et al. developed a miniaturized photoacoustic methane sensor with a detection limit of 92 part per billion (ppb) by using a 3.36 μm distributed feedback ICL [48]. A. Sampaolo et al. employed a 3.34 μm ICL for methane, ethane and propane detection using a compact quartz enhanced photoacoustic spectroscopy (QEPAS) sensor [49]. L. Dong et al. reported an ICL-based QEPAS sensor with vibrational-to-translational (V-T) relaxation self-calibration for atmospheric monitoring near a landfill [50].

In this work we report an ultra-highly sensitive CH_4 sensor based on a double-pass enhanced low-noise PAS cell and a room-temperature operating ICL having a center emission wavelength at Ø 3.3 μm. The PAS cell is designed in a differential resonator configuration to cancel the external noise and obtain a PAS signal with a high signal to noise ratio (SNR). An Al-coated concave reflector was positioned adjacent to a resonator to enhance the effective absorption. The operating pressure was optimized to achieve a PAS signal as large as possible. Water vapor (H_2O) was added into the gas as a promoter to increase the signal amplitude. With an integration time of 90 s a detection limit of 0.6 ppb for CH_4 was achieved.

2. Absorption line selection

A Nanoplus GmbH, continuous wave distributed feedback ICL mounted in a TO66 package emitting a single-mode laser beam was used as the light source to excite the photoacoustic signal. The temperature of the ICL chip was controlled by a thermoelectric cooler (TEC) enclosed in a 5×5×5 cm^3 cubic heat sink. Unlike traditional MIR sources, QCLs, do not require water or air cooling. An ICL operated at room temperature makes the sensor more compact and robust with a low power consumption. The emission wavelength of the ICL at different temperatures was measured using a Fourier-transform infrared spectrometer (FTIR, Thermofisher Nicolet IS50). Figure 1 shows the center laser emission wavenumber as a function of the injected current, when the temperature is varied from 20°C to 30°C. The current and temperature tuning coefficients of the ICL were measured to be −0.111 cm^{-1}/mA and −0.282 cm^{-1}/°C, respectively.

The methane main absorption bands are located in both the NIR and MIR spectral regions. In the NIR region, the typically absorption line selected is located at 6046.95 cm^{-1} (1.45×10^{-21} cm/molecule line strength) and can be targeted by a telecommunication diode laser [51]. Within

Optics EXPRESS

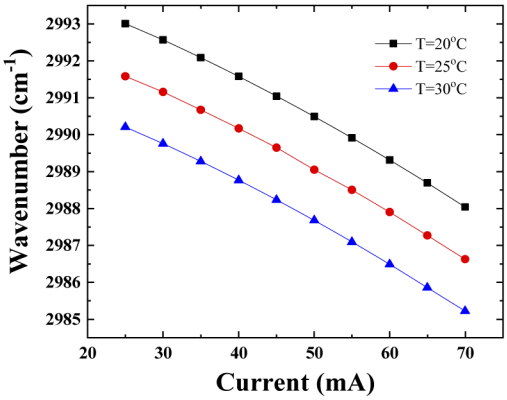

Fig. 1. Emission wavenumber of the ICL measured by Fourier-transform infrared spectrometer.

the emission spectral range of the ICL employed in this work a methane absorption line was selected at 2988.795 cm^{-1} with an intensity of 1.08×10^{-19} cm/molecule, which is two orders of magnitude stronger than the ones falling in the NIR region. The ICL optical power measured by a thermal power meter (Ophir Optronics 3A) at the target absorption line was 9.6 mW. Based on the HITRAN database [52], the absorption lines of CH_4 and of other possible interfering gas molecules in the spectral range from 2980 cm^{-1} to 3000 cm^{-1} are plotted in Fig. 2. As shown in the inset of Fig. 2, the selected CH_4 absorption line do not suffer from any interference due to absorption features of H_2O, C_3H_6, HCL and H_2O.

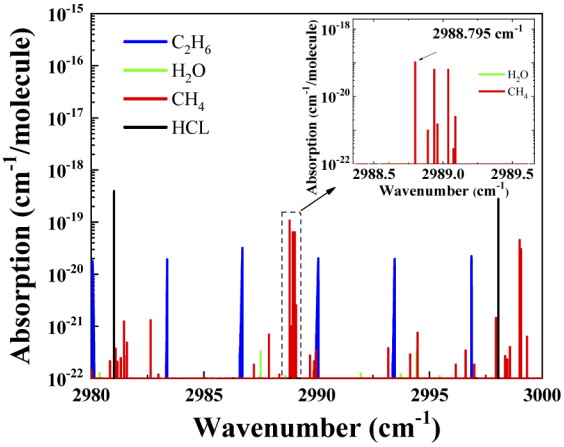

Fig. 2. Absorption lines of CH_4, C_3H_6, HCL and H_2O in the 2980-3000 cm^{-1} spectral range simulated using the HITRAN database.

3. PAS cell design and experimental setup

A differential photoacoustic cell was designed based on the well-known Helmholtz resonance [53]. The cell has two identical 90 mm-long cylindrical gas resonators with a diameter of 8 mm acting as signal and reference channel, respectively. Two buffer chambers with a length of 10 mm and a diameter of 20 mm are located at the two ends of the gas resonators. Two electret condenser microphones are imbedded into the walls in the middle of each resonator. The laser beam is

Optics EXPRESS

collimated and guided to one of the resonators. The other resonator is used as the reference. The gas flow noise and external acoustic disturbances are suppressed by using a differential preamplifier subtracting the reference from the signal. An Al-coated concave reflector with a reflectivity greater than 99% is positioned adjacent to the excited gas resonator. The reflector is mounted on a precision kinematic mount providing a double-pass absorption path in the gas resonator in order to enhance the photoacoustic signal amplitude. The fundamental longitudinal mode of the photoacoustic cell has a frequency of $f_0 = 1.8$ kHz with a quality factor of $Q_0 \sim 40$ at atmospheric pressure.

Figure 3 depicts the photoacoustic sensor setup. The temperature of the ICL is fixed at 25°C by a temperature controller (Wavelength LDTC 0520). A laser driver (ILX Lightwave LDX-3232) provides the current to the ICL source. A function generator (Stanford Research System DS345) allows laser current modulation. The injection current is modulated at a frequency of $f_0/2$, where f_0 corresponds to the fundamental resonance frequency of the PAS cell. A ramp signal is added to the sinusoidal modulation to scan the selected absorption line of the target gas. The photoacoustic signal detected by the microphones is first processed by a custom-made differential pre-amplifier and then fed to a lock-in amplifier (Stanford SR830) to demodulate the signal in $2f$ harmonic mode. The convenience in data processing, along with an improved SNR, gives the $2f$ second harmonic detection advantages for accurate and fast measurement. The time constant and filter slope of the lock-in amplifier are set to 1 s and 12 dB/otc, corresponding to a detection bandwidth of 0.25 Hz. The demodulated signal is recorded by a personal computer and the data are processed with a LabView-based software program. The target gas is flushed through the gas line and the PAS cell by employing a KNF vacuum pump. A Nafion humidifier is used to add water vapor to the gas samples. Two mass-flow controllers connected to the gas cylinders and a pressure controller (MKS Instruments) beyond the humidifier allow measurements to be performed at a controlled flow rate and pressure value.

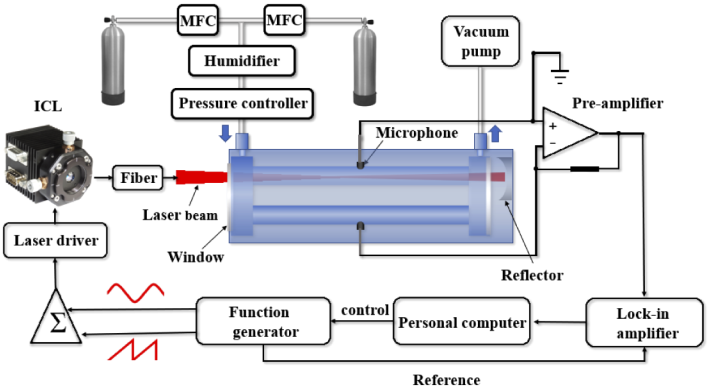

Fig. 3. Experimental setup of the CH_4 photoacoustic sensing system. ICL: interband cascade laser; MFC: mass flow controller. Σ: adder.

4. Results and discussion

4.1. Optimization of gas pressure and laser modulation depth

The gas pressure is a critical parameter in photoacoustic detection, since the parameters of the PAS cell, the V-T relaxation rate of the gas molecules and the intensity of the absorption spectra are pressure-dependent. An investigation on the influence of the operating pressure on the methane PAS signal was performed by using a 2 ppm CH_4/N_2 gas mixture and varying the gas pressure. Figure 4 shows the dependence of the PAS cell parameters and the PAS signal on

Optics EXPRESS

gas pressures. The gas pressure was changed from 178 Torr to 762 Torr (~ local atmospheric pressure). The resonance frequency of the PAS cell increased from 1782.75 Hz to 1804.63 Hz, corresponding to a frequency shift of 21.88 Hz. According to Fig. 4(b), the Q factor of the PAS cell changed from 23 to 46 when a pressure increases from 178 Torr to 762 Torr. In the same pressure range, the signal amplitude increased by ~ 2.7 times. This signal enhancement can be attributed to the increase of the Q factor of the PAS cell resonance and to the enhancement of the V-T relaxation rates. Based on these results, 762 Torr was selected as the optimum operating pressure value for the developed sensor system.

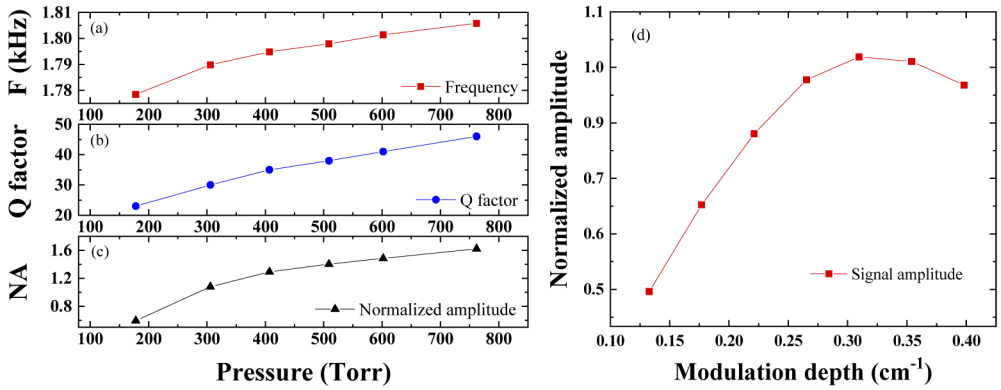

Fig. 4. Optimization of gas pressure and laser modulation depth. The PAS cell resonance frequency (a), Q factors (b) and normalized signal amplitudes (c) are plotted as the function of gas pressures. (d) Normalized signal amplitudes plotted as a function of the laser wavelength modulation depth. F: resonance frequency; NA: normalized amplitude.

According to the theory of wavelength modulation spectroscopy, the laser modulation depth can be optimized to maximize the QEPAS signal [54]. With this aim, the laser wavelength modulation depth was varied from 0.13 cm^{-1} to 0.4 cm^{-1} to evaluate the sensor performance at a selected 762 Torr pressure. A 2 ppm CH_4/N_2 mixture was flushed through the PAS cell with a flow rate of 100 standard cubic centimeters per minute (SCCM) at atmospheric pressure. The total gas flow rate value in the system was selected in order to avoid the occurrence of flow-related noise [55]. The normalized signal amplitude, namely the peak 2*f*-QEPAS signal normalized to the highest value, is plotted in Fig. 4(d) as a function of the modulation depth. The modulation depth providing the highest signal amplitude resulted to be 0.3 cm^{-1}.

4.2. PAS signal linearity and long-term stability

The sensor response to different CH_4 concentrations was then evaluated by operating the ICL at room temperature (25°C) with a modulation depth of 0.3 cm^{-1} and a pressure inside the PAS cell of 762 Torr. A gas dilution system (Beijing Sevenstar Electronics) with two mass flow controllers (MFCs) was employed to generate different CH_4 concentrations in N_2 mixtures. The PAS signal amplitudes as a function of the CH_4 concentration from 0 to 2 ppm are plotted in Fig. 5.

A linear fitting was carried out and the obtained R squared value of 0.999 confirms the linearity of the sensor response to the CH_4 concentration in the range under investigation. The 2*f* signal of a 2 ppm dry CH_4/N_2 gas mixture is shown in Fig. 6, obtained at a lock-in integration time of 1 s.

The laser wavelength was tuned from 2988.62 cm^{-1} to 2988.98 cm^{-1} to cover the selected CH_4 absorption line. At 2988.80 cm^{-1} a peak signal of 7.8×10^{-5} V was measured, while the noise recorded at 2988.36 cm^{-1}, far from the absorption peak, was ~1.7×10^{-7} V, leading to a signal to noise ratio of ~ 460, corresponding to an ultimate detection limit of ~ 4 ppb. With an excitation power of 9.6 mW and detection bandwidth of 0.25 Hz, a normalized noise

Optics EXPRESS

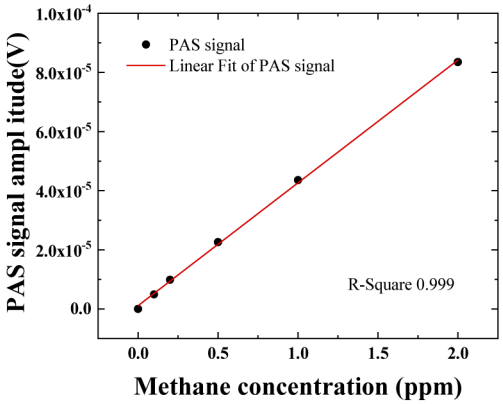

Fig. 5. Photoacoustic signal amplitudes as a function of CH_4 concentrations from 0 to 2 ppm (black dots) and linear fit (red solid line). The slope of the linear fit is ~4.15×10^{-5} V/ppm.

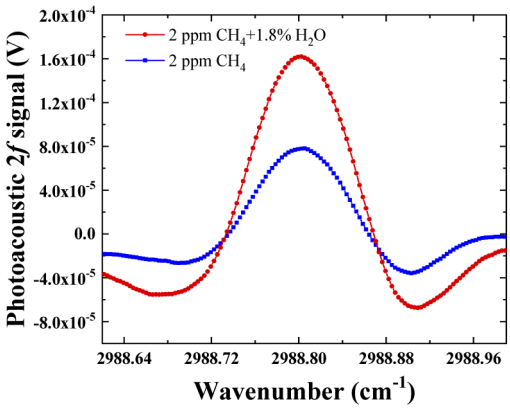

Fig. 6. Photoacoustic 2*f* signal for 2 ppm dry CH_4/N_2 gas mixture and 2 ppm CH_4/N_2 gas mixture containing 1.8% H_2O vapor, at a lock-in integration time of 1 s.

equivalent absorption coefficient (NNEA) of ~1.23×10^{-9} W·cm^{-1}·Hz$^{-1/2}$ was achieved. This NNEA is slightly better than the methane sensor by quartz enhanced photoacoustic spectroscopy [50,56]. The improvement can be attributed to the low noise generated from differential acoustic configuration and signal improvement induced by the double optical pass.

An Allan-Werle deviation analysis allows the determination of how long the optical sensor signals can be averaged in order to improve the detection sensitivity [57,58]. To assess the long-term stability, the laser wavelength was tuned away from the CH_4 absorption line at 2988.36 cm^{-1}. A 2 ppm CH_4/N_2 gas mixture was fed to the PAS cell with a gas flow rate of 100 SCCM. The lock-in amplifier continuously recorded the data from the sensor with an integration time of 1 s and a slope of 12 dB/octave. The calculated CH_4 detection limit as a function of integration time was plotted in Fig. 7, basing on the Allan-Werle deviation. Within the integration time of 90 s, the standard deviation decreased down to ~ 5×10^{-8} V corresponding to a ~1.2 ppb detection limit.

Optics EXPRESS

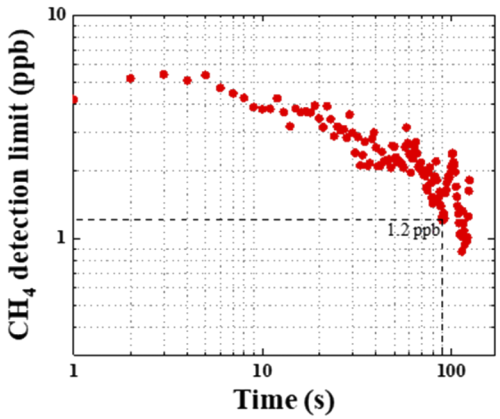

Fig. 7. CH_4 detection limit as a function of the integration time, based on Allan-Werle variance analysis.

4.3. Methane V-T relaxation enhancement

Water vapor acts as a promoter of the energy relaxation processes for CH_4. To investigate this effect, H_2O was added to the gas mixture. The water concentration was controlled by the nafion humidifier which was the same as the one used in [59]. Considering a mixture of methane in a matrix composed of nitrogen and water vapor, in a simplified one-stage collision between molecules, the obtained photoacoustic signal S in a wet CH_4/N_2 gas mixture consists of two contributions: the collision of CH_4 and N_2 molecules described by S_{N2} as well as the collision of CH_4 and H_2O molecules described by S_{H2O}. Therefore, the CH_4 PAS signal in a humidified mixture of N_2 and H_2O can be expressed as follows [60]:

$$S = S_{N_1} + S_{H_1O} \approx S_{N_i}\left[1 + \frac{\eta - 1}{\sqrt{1 + \left(\frac{2\pi \cdot f \cdot P_0\tau_0}{P_{B,O}}\right)^2}}\right], \tag{2}$$

where η is the ratio of PAS signal of CH_4/N_2 gas mixture with saturated H_2O vapor to PAS signal of CH_4/N_2 gas mixture with no H_2O; f is the modulation frequency, $P_0\tau_0$ is the vibration to translation (V-T) relaxation constant, P_{H2O} is the partial pressure of H_2O in CH_4/N_2 gas mixture. As shown in Fig. 6, when adding 1.8% H_2O to the CH_4/N_2 gas mixture the photoacoustic peak signal was ~1.6×10^{-4} V, doubled with respect to the dry mixture, while the noise level did not change. As a result, an ultimate detection sensitivity of 0.6 ppb at 90 s integration time can be achieved by using a CH_4/N_2 gas mixture with 1.8% H_2O. A detailed investigation of the water impact on methane PAS signals can be found in [61].

5. Conclusions

A highly sensitive CH_4 sensor was demonstrated, implementing an interband cascade laser operating at 3.3 μm and a low-noise differential PAS cell. An Al-coated reflector was positioned at the end of the PAS cell to allow double optical pass absorption and enhance the signal amplitude. The differential structure of the PAS cell combined with a custom-made differential pre-amplifier effectively suppresses the background noise. The influence on the PAS signal of wavelength modulation depth and the gas mixture pressures was investigated in order to optimize the sensor performance. With a 1 s integration time a 1σ standard deviation of ~1.7×10^{-7} V was achieved. A long-term stability analysis on the sensor shows that an integration time of 90 s allows a

Optics EXPRESS

sensitivity of ~1.2 ppb can be reached. Moreover, a signal enhancement of ~ 2 times is provided by a 1.8% H_2O vapor concentration added to the dry mixture. By employing all the optimized parameters, i.e. laser modulation depth, operating gas pressure, lock-in integration time and H_2O vapor concentration, a detection limit of ~0.6 ppb can be achieved.

The detection sensitivity obtained by the developed PAS sensor was comparable to mid-infrared methane sensors based on tunable diode laser absorption spectroscopy [40,41,62]. However, no optical detector was required in the PAS system, resulting in a simpler sensor structure. The use of an ICL as the light source operated at room temperature allowed avoiding the use of a water or cooling system. Therefore, the reported sensor is particularly suitable for future work focusing on the development of a portable and light-weight sensor for CH_4 monitoring in ambient air.

Funding

National Natural Science Foundation of China (61675092, 61705086, 61601404, 61771222); Natural Science Foundation of Guangdong Province (2020B1515020024, 2016A030313079, 2016A030311019, 2017A030313375, 2019A1515011380); Key-Area Research and Development Program of Guangdong Province (2019B010138004, 2017A010102006, 2015B010125007); Project of Guangzhou Industry Leading Talents (CXLJTD-201607); Planned Science & Technology Project of Guangzhou (201707010396, 2016B010111003); Aeronautical Science Foundation of China (201708W4001, 201808W4001); Joint fund of pre-research for equipment, Ministry of Education of the People's Republic of China (6141A02022124); Open foundation of CEPREI (NO. 19D09); Foundation for Distinguished Young Talents in Higher Education of Guangdong (2018KQNCX009); Fundamental Research Funds for the Central Universities (21619402, 11618413); State Key Laboratory of Applied Optics (SKLAO-201914); National Science Foundation (ERC MIRTHE award, No. R3H685); Welch Foundation (C-0586); H2020 Marie Skłodowska-Curie Actions (No. 860808).

Acknowledgments

The authors would like to thank Prof. Lei Dong from Shanxi University for the helpful discuss to improve the manuscript. Frank Tittel acknowledges the financial support from the US National Science Foundation (NSF) ERC MIRTHE award, a NSF NeTS Large "ASTRO" award (No. R3H685) and a grant C-0586 from the Welch Foundation. The authors from Dipartimento Interateneo di Fisica di Bari acknowledge the financial support from the European Union's Horizon 2020 research and innovation programme under the Marie Skłodowska-Curie project OPTAPHI, grant No. 860808 and from THORLABS GmbH within the joint-research laboratory.

Disclosures

The authors declare no conflicts of interest.

References

1. IPCC Fourth Assessment Report: Climate Change 2007; 2.10.2 Direct Global Warming Potentials, 2007, Intergovernmental Panel on Climate Change.
2. M. W. Sigrist, "Trace gas monitoring by laser photoacoustic spectroscopy and related techniques," Rev. Sci. Instrum. **74**(1), 486–490 (2003).
3. P. Patimisco, G. Scamarcio, and V. Spagnolo, "Quartz-enhanced photoacoustic spectroscopy: a review," Sensors **14**(4), 6165–6206 (2014).
4. A. Miklós, P. Hess, and Z. Bozóki, "Application of acoustic resonators in photoacoustic trace gas analysis and metrology," Rev. Sci. Instrum. **72**(4), 1937–1955 (2001).
5. R. Bernhardt, G. D. Santiago, V. B. Slezak, A. Peuriot, and M. G. González, "Differential LED-excited resonant NO_2 photoacoustic system," Sens. Actuators, B **150**(2), 513–516 (2010).
6. J. Kottmann, J. M. Rey, and M. W. Sigrist, "Mid-Infrared photoacoustic detection of glucose in human skin: towards non-invasive diagnostics," Sensors **16**(10), 1663–1677 (2016).

Optics EXPRESS

7. J. Li, W. Chen, and B. Yu, "Recent progress on infrared photoacoustic spectroscopy techniques," Appl. Spectrosc. Rev. **46**(6), 440–471 (2011).
8. Y. Cao, W. Jin, H. L. Ho, and J. Ma, "Miniature fiber-tip photoacoustic spectrometer for trace gas detection," Opt. Lett. **38**(4), 434–436 (2013).
9. Z. Gong, K. Chen, Y. Yang, X. Zhou, W. Peng, and Q. Yu, "High-sensitivity fiber-optic acoustic sensor for photoacoustic spectroscopy based traces gas detection," Sens. Actuators, B **247**, 290–295 (2017).
10. S. Zhou and D. Iannuzzi, "A fiber-tip photoacoustic sensor for in situ trace gas detection," Rev. Sci. Instrum. **90**(2), 023102 (2019).
11. K. Chen, Z. Yu, Q. Yu, M. Guo, Z. Zhao, C. Qu, Z. Gong, and Y. Yang, "Fast demodulated white-light interferometry-based fiber-optic Fabry–Perot cantilever microphone," Opt. Lett. **43**(14), 3417–3420 (2018).
12. T. Tomberg, T. Hieta, M. Vainio, and L. Halonen, "Cavity-enhanced cantilever-enhanced photo-acoustic spectroscopy," Analyst **144**(7), 2291–2296 (2019).
13. V. Koskinen, J. Fonsen, K. Roth, and J. Kauppinen, "Progress in cantilever enhanced photoacoustic spectroscopy," Vib. Spectrosc. **48**(1), 16–21 (2008).
14. A. A. Kosterev, Y. A. Bakhirkin, R. F. Curl, and F. K. Tittel, "Quartz-enhanced photoacoustic spectroscopy," Opt. Lett. **27**(21), 1902–1904 (2002).
15. M. Giglio, A. Zifarelli, A. Sampaolo, G. Menduni, A. Elefante, R. Blanchard, C. Pfluegl, M. F. Witinski, D. Vakhshoori, H. Wu, V. M. N. Passaro, P. Patimisco, F. K. Tittel, L. Dong, and V. Spagnolo, "Broadband detection of methane and nitrous oxide using a distributed-feedback quantum cascade laser array and quartz-enhanced photoacoustic sensing," Photoacoustics **17**, 100159 (2020).
16. L. Dong, A. A. Kosterev, D. Thomazy, and F. K. Tittel, "QEPAS spectrophones: design, optimization, and performance," Appl. Phys. B: Lasers Opt. **100**(3), 627–635 (2010).
17. Y. Ma, Y. He, P. Patimisco, A. Sampaolo, S. Qiao, X. Yu, F. K. Tittel, and V. Spagnolo, "Ultra-high sensitive trace gas detection based on light-induced thermoelastic spectroscopy and a custom quartz tuning fork," Appl. Phys. Lett. **116**(1), 011103 (2020).
18. W. Ren, W. Jiang, N. P. Sanchez, P. Patimisco, V. Spagnolo, C. Zah, F. Xie, L. C. Hughes, R. J. Griffin, and F. K. Tittel, "Hydrogen peroxide detection with quartz-enhanced photoacoustic spectroscopy using a distributed-feedback quantum cascade laser," Appl. Phys. Lett. **104**(4), 041117 (2014).
19. H. Zheng, L. Dong, A. Sampaolo, H. Wu, P. Patimisco, X. Yin, W. Ma, L. Zhang, W. Yin, V. Spagnolo, S. Jia, and F. K. Tittel, "Single-tube on-beam quartz-enhanced photoacoustic spectroscopy," Opt. Lett. **41**(5), 978–981 (2016).
20. Q. Zhang, J. Chang, Z. Cong, Y. Feng, Z. Wang, and J. Sun, "Scanned-wavelength intra-cavity QEPAS sensor with injection seeding technique for C2H2 detection," Opt. Laser Technol. **120**, 105751 (2019).
21. M. Giglio, A. Elefante, P. Patimisco, A. Sampaolo, F. Sgobba, H. Rossmadl, V. Mackowiak, H. Wu, F. K. Tittel, L. Dong, and V. Spagnolo, "Quartz-enhanced photoacoustic sensor for ethylene detection implementing optimized custom tuning fork-based spectrophone," Opt. Express **27**(4), 4271–4280 (2019).
22. A. Sampaolo, P. Patimisco, M. Giglio, M. S. Vitiello, H. E. Beere, D. A. Ritchie, G. Scamarcio, and V. Spagnolo, "Improved tuning fork for terahertz quartz-enhanced photoacoustic spectroscopy," Sensors **16**(4), 439 (2016).
23. H. Wu, L. Dong, H. Zheng, Y. Yu, W. Ma, L. Zhang, W. Yin, L. Xiao, S. Jia, and F. K. Tittel, "Beat frequency quartz-enhanced photoacoustic spectroscopy for fast and calibration-free continuous trace-gas monitoring," Nat. Commun. **8**(1), 15331 (2017).
24. L. Dong, C. Li, N. P. Sanchez, A. K. Gluszek, R. J. Griffin, and F. K. Tittel, "Compact CH_4 sensor system based on a continuous-wave, low power consumption, room temperature interband cascade laser," Appl. Phys. Lett. **108**(1), 011106 (2016).
25. Y. Zhang, W. Gao, Z. Song, Y. An, L. Li, Z. Song, W. Yu, and Y. Wang, "Design of a novel gas sensor structure based on mid-infrared absorption spectrum," Sens. Actuators, B **147**(1), 5–9 (2010).
26. Y. Ma, Y. He, Y. Tong, X. Yu, and F. K. Tittel, "Quartz-tuning-fork enhanced photothermal spectroscopy for ultra-high sensitive trace gas detection," Opt. Express **26**(24), 32103–32110 (2018).
27. J. Karhu, T. Tomberg, F. S. Vieira, G. Genoud, V. Hänninen, M. Vainio, M. Metsälä, T. Hieta, S. Bell, and L. Halonen, "Broadband photoacoustic spectroscopy of CH_4 14 with a high-power mid-infrared optical frequency comb," Opt. Lett. **44**(5), 1142–1145 (2019).
28. M. Lassen, L. Lamard, Y. Feng, A. Peremans, and J. C. Petersen, "Off-axis quartz-enhanced photoacoustic spectroscopy using a pulsed nanosecond mid-infrared optical parametric oscillator," Opt. Lett. **41**(17), 4118–4121 (2016).
29. V. Spagnolo, P. Patimisco, S. Borri, G. Scamarcio, B. E. Bernacki, and J. Kriesel, "Part-per-trillion level SF_6 detection using a quartz enhanced photoacoustic spectroscopy-based sensor with single-mode fiber-coupled quantum cascade laser excitation," Opt. Lett. **37**(21), 4461–4463 (2012).
30. J. P. Waclawek, H. Moser, and B. Lendl, "Compact quantum cascade laser based quartz-enhanced photoacoustic spectroscopy sensor system for detection of carbon disulfide," Opt. Express **24**(6), 6559–6571 (2016).
31. J. S. Li, B. Yu, H. Fischer, W. Chen, and A. P. Yalin, "Contributed Review: Quantum cascade laser based photoacoustic detection of explosives," Rev. Sci. Instrum. **86**(3), 031501 (2015).
32. M. Giglio, P. Patimisco, A. Sampaolo, A. Zifarelli, R. Blanchard, C. Pfluegl, M. F. Witinski, D. Vakhshoori, F. K. Tittel, and V. Spagnolo, "Nitrous oxide quartz-enhanced photoacoustic detection employing a broadband distributed-feedback quantum cascade laser array," Appl. Phys. Lett. **113**(17), 171101 (2018).

Optics EXPRESS

33. H. Wu, X. Yin, L. Dong, Z. Jia, J. Zhang, F. Liu, W. Ma, L. Zhang, W. Yin, L. Xiao, S. Jia, and F. K. Tittel, "Ppb-level nitric oxide photoacoustic sensor based on a mid-IR quantum cascade laser operating at 52°C," Sens. Actuators, B **290**, 426–433 (2019).
34. Z. Li, C. Shi, and W. Ren, "Mid-infrared multimode fiber-coupled quantum cascade laser for off-beam quartz-enhanced photoacoustic detection," Opt. Lett. **41**(17), 4095–4098 (2016).
35. T. Berer, M. Brandstetter, A. Hochreiner, G. Langer, W. Märzinger, P. Burgholzer, and B. Lendl, "Remote mid-infrared photoacoustic spectroscopy with a quantum cascade laser," Opt. Lett. **40**(15), 3476–3479 (2015).
36. K. Krzempek, A. Hudzikowski, A. Głuszek, G. Dudzik, K. Abramski, G. Wysocki, and M. Nikodem, "Multi-pass cell-assisted photoacoustic/photothermal spectroscopy of gases using quantum cascade laser excitation and heterodyne interferometric signal detection," Appl. Phys. B: Lasers Opt. **124**(5), 74 (2018).
37. S. Zhou, L. Xu, L. Zhang, T. He, N. Liu, Y. Liu, B. Yu, and J. Li, "External cavity quantum cascade laser-based QEPAS for chlorodifluoromethane spectroscopy and sensing," Appl. Phys. B: Lasers Opt. **125**(7), 125 (2019).
38. Y. He, Y. Ma, Y. Tong, X. Yu, and F. K. Tittel, "Ultra-high sensitive light-induced thermoelastic spectroscopy sensor with a high Q-factor quartz tuning fork and a multipass cell," Opt. Lett. **44**(8), 1904–1907 (2019).
39. X. Yin, H. Wu, L. Dong, B. Li, W. Ma, L. Zhang, W. Yin, L. Xiao, S. Jia, and F. K. Tittel, "Ppb-level so$_2$ photoacoustic sensors with a suppressed absorption–desorption effect by using a 7.41 μm external-cavity quantum cascade laser," ACS Sens. **5**(2), 549–556 (2020).
40. C. Zheng, W. Ye, N. P. Sanchez, A. K. Gluszek, A. J. Hudzikowski, C. Li, L. Dong, R. J. Griffin, and F. K. Tittel, "Infrared dual-gas CH_4/C_2H_6 sensor using two continuous-wave interband cascade lasers," IEEE Photonics Technol. Lett. **28**(21), 2351–2354 (2016).
41. W. Ye, C. Li, C. Zheng, N. P. Sanchez, A. K. Gluszek, A. J. Hudzikowski, L. Dong, R. J. Griffin, and F. K. Tittel, "Mid-infrared dual-gas sensor for simultaneous detection of methane and ethane using a single continuous-wave interband cascade laser," Opt. Express **24**(15), 16973–16985 (2016).
42. R. Q. Yang, "Infrared laser based on intersubband transitions in quantum wells," Superlattices Microstruct. **17**(1), 77–83 (1995).
43. I. Vurgaftman, R. Weih, M. Kamp, J. R. Meyer, C. L. Canedy, C. S. Kim, M. Kim, W. W. Bewley, C. D. Merritt, J. Abell, and S. Höfling, "Interband cascade lasers," J. Phys. D: Appl. Phys. **48**(12), 123001 (2015).
44. J. Hillbrand, M. Beiser, A. M. Andrews, H. Detz, R. Weih, A. Schade, S. Höfling, G. Strasser, and B. Schwarz, "Picosecond pulses from a mid-infrared interband cascade laser," Optica **6**(10), 1334–1337 (2019).
45. Z. Wang, Q. Wang, J. Y. L. Ching, J. C. Y. Wu, G. Zhang, and W. Ren, "A portable low-power QEPAS-based CO_2 isotope sensor using a fiber-coupled interband cascade laser," Sens. Actuators, B **246**, 710–715 (2017).
46. A. Loh and M. Wolff, "High resolution spectra of 13C ethane and propane isotopologues photoacoustically measured using interband cascade lasers near 3.33 and 3.38 μm, respectively," J. Quant. Spectrosc. Radiat. Transfer **227**, 111–116 (2019).
47. M. Lassen, D. B. Harder, A. Brusch, O. S. Nielsen, D. Heikens, S. Persijn, and J. C. Petersen, "Photo-acoustic sensor for detection of oil contamination in compressed air systems," Opt. Express **25**(3), 1806–1814 (2017).
48. J. Rouxel, J. G. Coutard, S. Gidon, O. Lartigue, S. Nicoletti, B. Parvitte, R. Vallon, V. Zéninari, and A. Glière, "Miniaturized differential Helmholtz resonators for photoacoustic trace gas detection," Sens. Actuators, B **236**, 1104–1110 (2016).
49. A. Sampaolo, S. Csutak, P. Patimisco, M. Giglio, G. Menduni, V. Passaro, F. K. Tittel, M. Deffenbaugh, and V. Spagnolo, "Methane, ethane and propane detection using a compact quartz enhanced photoacoustic sensor and a single interband cascade laser," Sens. Actuators, B **282**, 952–960 (2019).
50. H. Wu, L. Dong, X. Yin, A. Sampaolo, P. Patimisco, W. Ma, L. Zhang, W. Yin, L. Xiao, V. Spagnolo, and S. Jia, "Atmospheric CH_4 measurement near a landfill using an ICL-based QEPAS sensor with VT relaxation self-calibration," Sens. Actuators, B **297**, 126753 (2019).
51. R. Y. Cui, L. Dong, H. P. Wu, L. T. Xiao, S. T. Jia, W. D. Chen, and F. K. Tittel, "3D–printed miniature fiber-coupled multi-pass cell with dense spot pattern for ppb-level methane detection using a near-IR diode laser," submitted to Anal. Chem. (2020).
52. Http://hitran.org.
53. T. Starecki, "Windowless open photoacoustic Helmholtz cell," Acta Phys. Pol., A **114**(6A), A-211–A-216 (2008).
54. P. Patimisco, A. Sampaolo, Y. Bidaux, A. Bismuto, M. Scott, J. Jiang, A. Muller, J. Faist, F. K. Tittel, and V. Spagnolo, "Purely wavelength- and amplitude-modulated quartz-enhanced photoacoustic spectroscopy," Opt. Express **24**(23), 25943–25954 (2016).
55. H. Zheng, L. Dong, X. Yin, X. Liu, H. Wu, L. Zhang, W. Ma, W. Yin, and S. Jia, "Ppb-level QEPAS NO_2 sensor by use of electrical modulation cancellation method with a high power blue LED," Sens. Actuators, B **208**, 173–179 (2015).
56. Y. Li, R. Wang, F. K. Tittel, and Y. Ma, "Sensitive methane detection based on quartz-enhanced photoacoustic spectroscopy with a high-power diode laser and wavelet filtering," Opt. Laser. Eng. **132**, 106155 (2020).
57. H. Zheng, Y. Liu, H. Lin, B. Liu, X. Gu, D. Li, B. Huang, Y. Wu, L. Dong, W. Zhu, J. Tang, H. Guan, H. Lu, Y. Zhong, J. Fang, Y. Luo, J. Zhang, J. Yu, Z. Chen, and F. K. Tittel, "Quartz-enhanced photoacoustic spectroscopy employing pilot line manufactured custom tuning forks," Photoacoustics **17**, 100158 (2020).
58. M. Giglio, P. Patimisco, A. Sampaolo, G. Scamarcio, F. K. Tittel, and V. Spagnolo, "Allan deviation plot as a tool for quartz-enhanced photoacoustic sensors noise analysis," IEEE Trans. Ultrason., Ferroelect., Freq. Contr. **63**(4), 555–560 (2016).

Optics EXPRESS

59. H. Lin, Z. Huang, R. Kan, H. Zheng, Y. Liu, B. Liu, L. Dong, W. Zhu, J. Tang, J. Yu, Z. Chen, and F. K. Tittel, "Application of Micro Quartz Tuning Fork in Trace Gas Sensing by Use of Quartz-Enhanced Photoacoustic Spectroscopy," Sensors **19**(23), 5240 (2019).
60. X. Yin, L. Dong, H. Zheng, X. Liu, H. Wu, Y. Yang, W. Ma, L. Zhang, W. Yin, L. Xiao, and S. Jia, "Impact of humidity on quartz-enhanced photoacoustic spectroscopy based CO detection using a near-IR telecommunication diode laser," Sensors **16**(2), 162 (2016).
61. A. Elefante, G. Menduni, H. Rossmadl, V. Mackowiak, M. Giglio, A. Sampaolo, P. Patimisco, V. M. N. Passaro, and V. Spagnolo, "Environmental monitoring of methane with quartz-enhanced photoacoustic spectroscopy exploiting an electronic hygrometer to compensate the H_2O influence on the sensor signal," Sensors **20**(10), 2935 (2020).
62. C. Zheng, W. Ye, N. P. Sanchez, C. Li, L. Dong, Y. Wang, R. J. Griffin, and F. K. Tittel, "Development and field deployment of a mid-infrared methane sensor without pressure control using interband cascade laser absorption spectroscopy," Sens. Actuators, B **244**, 365–372 (2017).

159.226.165.15 {ts '2021-04-20 04:23:26'}